DALTON

# Preparation, characterisation and properties of Groups VIII and IB metal nanoparticles †

**Robert W. Devenish,[a] Terence Goulding,[b] Brian T. Heaton[b] and Robin Whyman *[,b]**

[a] *Department of Materials Science and Engineering, University of Liverpool, PO Box 147, Liverpool L69 3BX, UK*

[b] *Department of Chemistry, University of Liverpool, PO Box 147, Liverpool L69 3BX, UK*

Vapour synthesis techniques have been used to prepare nanoparticulate dispersions of ruthenium, rhodium, palladium, platinum, silver and gold in non-aqueous solvents. The dimensions of these solvent-stabilised particles, which can be controlled within the 1–3 nm size regime, effectively encompass the areas of molecular chemistry (as typified by high-nuclearity metal clusters) and the smaller colloidal metals. The nanostructures have been characterised by high-resolution transmission electron microscopy and evidence for face-centred cubic (f.c.c.) octahedral, f.c.c. cuboctahedral and icosahedral metal particles obtained; quasi-molten states have also been observed in a number of these systems. In addition to discrete particles, larger aggregates of the small primary particles have been observed, some of which appear to be organometallic in nature. Gold nanoparticles differ from those of the Group VIII metals in exhibiting unusual time and concentration-dependent behaviour. A regime of preparative conditions under which 1–3 nm size gold particles, which are stable with respect to aggregation as a function of time, is defined. Some preliminary results of attempts to use laser mass spectrometry as a rapid method for the molecular mass determination of some of these materials are also described.

One of the reasons for the considerable current interest in small-particle research is because such materials fall into that intermediate state of matter between molecular and bulk, and frequently display unusual physical (structural, electronic, magnetic and optical) and chemical (catalytic) properties.[1] In the context of discrete metal clusters, crystallographically characterised examples now exist which range in nuclearity between those containing 3 and up to 44 metal atoms, *e.g.* $[Ni_{38}Pt_6(CO)_{48}H_{6-n}]^{n-}$.[2] Other evidence, including EXAFS (extended X-ray absorption fine structure), has been provided in support of the formulation of a series of $M_{55}L_{12}Cl_x$ (L = $PPh_3$) clusters and for the formation of a family of giant palladium clusters containing 309 and 561 metal atoms.[3,4] The natural progression from a cluster to the smallest colloidal metal particle may occur in a continuous fashion although the situation is complicated by the fact that high-nuclearity clusters are usually prepared and studied in organic solvents whereas, with few exceptions,[5] typical colloidal metal preparations involve the reduction of aqueous solutions of metal salts. Such solutions can thus contain a variety of counter ions, the presence and effects of which are usually neither considered nor understood. In addition metal colloids are frequently protected from aggregation by the addition of various stabilising 'ligands', *e.g.* polymers and dispersing agents. Co-ordination chemistry, in a variety of guises, has therefore an important, and perhaps hitherto largely unrecognised, role to play in the stabilisation of colloidal metals.

The main hindrances to progress in this region which encompasses molecular chemistry and the colloidal state have been the paucity of relatively simple, reproducible and *generally* applicable synthetic procedures together with difficulties in structural characterisation. In order to address this problem of synthesis we have applied recent developments in metal vapour synthesis (MVS)[6,7] and have demonstrated that the electron-beam evaporation of Group VIII and Group IB metals followed by co-condensation with the vapours of organic solvents at 77 K leads, after warm-up, to the formation of solvent-stabilised metal nanoparticles, the dimensions of which can be controlled within this critical intermediate 1–5 nm particle size range. In the additional presence of dispersing agents particles in even narrower size ranges (1–3 nm) can be generated and stabilised. Characterisation of the nanoparticles so produced has been effected primarily using high-resolution transmission electron microscopy (HRTEM), the details of which are described herein. In addition we have begun to explore the potential of other techniques such as matrix-assisted laser desorption ionisation time-of-flight mass spectrometry (MALDI-TOF) and some preliminary results are described.

† Basis of the presentation given at Dalton Discussion No. 1, 3rd–5th January 1996, University of Southampton, UK.

## Experimental

### Preparation of solvent-stabilised metal nanoparticles

Solutions containing metal nanoparticles were prepared by metal-vapour synthesis techniques using a commercial positive-hearth electrostatically focused electron-beam rotary metal-atom reactor (Torrovap Industries, Inc., Ontario, Canada). Typically 0.1 g platinum was evaporated under a dynamic vacuum of *ca.* $5 \times 10^{-7}$ Torr (*ca.* $6.65 \times 10^{-5}$ Pa) over 3 h and co-condensed at 77 K with *ca.* 200 $cm^3$ degassed, dried butan-2-one (ethyl methyl ketone). After slow warm-up and melting the resultant brown liquid was transferred under anaerobic conditions from the reactor flask into a Schlenk receiver vessel. In addition to simple metal–solvent combinations, dispersing agents were also added with the purpose of enhancing the stability of the smallest particles. The dispersing agents used, KD1 and KD2, are examples of the Hypermer KD range of polymeric dispersants which are marketed under the Solsperse tradename by Zeneca Colours. These were normally introduced at *ca.* 0.1 wt.% concentration in ethyl methyl ketone (30–40 $cm^3$) at the conclusion of the evaporation procedure while the metal–solvent matrix was still frozen. The mixture was then allowed to warm slowly to room temperature, with slow rotation (30 rpm) of the reactor flask to ensure good mixing.

**Table 1** Preparations of solvent-stabilised metal nanoparticles

| | Solvent | | | | | |
|---|---|---|---|---|---|---|
| | Ethyl methyl ketone | | | | | |
| Metal | Alone | +KD1 | +KD2 | Acetone–water (4:1) | Toluene | Methylcyclohexane |
| Ru | √ | √ | √ | — | — | — |
| Rh | √ | √ | √ | — | √ | — |
| Pd | √ | √ | √ | — | — | — |
| Pt | √ | √ | √ | √ | — | √ |
| Ag | √ | √ | √ | — | — | — |
| Au | √ | √ | √ | √ | √ | √ |

After backfilling with dry dinitrogen, the usually brown liquids were transferred to the Schlenk receiver flask and stored in an inert atmosphere. The range of metal–solvent–dispersing agent combinations investigated is summarised in Table 1.

### High-resolution transmission electron microscopy

Phase-contrast images of the nanoparticles were obtained with a top-entry JEOL 2000EX electron microscope operating at an accelerating voltage of 200 kV (point resolution 0.21 nm). Specimens for examination were prepared by evaporation of one or two drops of the solutions containing the metal nanoparticles on to lacey carbon films supported on standard copper grids. A range of supports was also used in order to enhance particle visibility, principally by overcoming the background speckle contrast from carbon films. The supports included MgO smoke cubes, ultrathin (10 nm) platelets of MgO (ex-USC, Japan) and silica microspheres of diameter *ca.* 250 nm (courtesy of Professor A. K. Datye, University of New Mexico, USA).

### Matrix-assisted laser desorption ionisation time-of-flight mass spectrometry

The MALDI spectra were obtained courtesy of Kratos Analytical using a Kratos Kompact MALDI 3 instrument with reflectron attachment. The spectrum of the gold–ethyl methyl ketone sample was obtained without the use of a matrix; sinapinic acid [3-(4-hydroxy-3,5-dimethoxyphenyl)prop-2-enoic acid] was used as the matrix for the palladium sample.

## Results and Discussion

### Preparation of solvent-stabilised metal nanoparticles

In preliminary work in this area we demonstrated that ethyl methyl ketone was a particularly appropriate solvent/reaction medium for the preparation of solvent-stabilised palladium nanoparticles by the MVS route.[8] The additional presence of a dispersing agent such as KD1 was found to enhance the stability of the particles, particularly at higher metal concentrations, towards aggregation during long-term storage. Most of our current experimental approach incorporating other metals has concentrated on this solvent–dispersing agent combination. Nevertheless we have conducted a brief examination of different solvents with other metals and the range of metal–solvent–dispersing agent combinations investigated is summarised in Table 1.

In general at least duplicate preparations of a particular combination were carried out and samples were prepared at both low and high concentrations within the nominal range (based on mass of metal evaporated) of 0.2–6.0 g $l^{-1}$. This is equivalent to molarity ranges of $7.0 \times 10^{-3}$–$3.0 \times 10^{-2}$ and $3.5 \times 10^{-3}$–$1.5 \times 10^{-2}$ for second- and third-row metals respectively. However, as indicated above, this is only a nominal concentration range and the real values are somewhat less. This is because the MVS procedure is less than 100% efficient in respect of the amount of metal converted into useful products. In general, within the configuration of the rotary metal-atom reactor, approximately 60–70% of the metal evaporated is converted into discrete nanoparticles, the remainder being distributed as bulk metal around the electron-gun shields and on the walls of the reactor flask beyond the limits of condensation of the solvent vapour.

A general feature of the preparations of solvent-stabilised platinum-group metal nanoparticles is the formation of brown solutions with colour intensities proportional to the amount of metal evaporated and the shade of brown varying slightly with the nature of the metal. For example, ruthenium-containing solutions appear yellow-brown, rhodium reddish brown and palladium and platinum both dark brown. In general ethyl methyl ketone solutions are stable with respect to storage under dinitrogen over relatively short periods (days to weeks) but change slowly over 3–6 months with the gradual deposition of solid and a slight reduction in intensity of the colour of the supernatant liquid. The use of dispersing agents enhances the stability of the solutions and reduces the rate of deposition of solids. In terms of the different solvents used the stability of the nanoparticles with respect to long-term storage lies in the order ethyl methyl ketone > acetone–water > toluene > methylcyclohexane.

Comparison of nanoparticles of the coinage-group metals with platinum-group metals highlights some significant differences. Silver nanoparticles obtained by the co-condensation of Ag with the ketone seemed particularly unstable with respect to flocculation/precipitation, irrespective of the presence of dispersing agents. Although not resulting in precipitation, solutions of gold nanoparticles displayed an unusual concentration-dependent aggregation phenomenon which could be monitored by a combination of optical spectroscopy and HRTEM (see below).

In general, factors which qualitatively control the particle sizes include the mass of metal evaporated, the rate of evaporation, the metal/co-condensate ratio and the co-condensation temperature. Low values of all of these favour the formation of smaller particles. Factors such as the rate of matrix warm-up and warm-up under a static vacuum *vs.* an atmosphere of dinitrogen can also be significant.

### High-resolution transmission electron microscopy

In preliminary HRTEM characterisation work with palladium–ethyl methyl ketone nanoparticles we demonstrated (*i*) that particles in the size range 2–5 nm were present and (*ii*) that when the preparation was carried out in the presence of KD1 the size distribution was further narrowed into the range 2–3 nm. This has now been shown to be a general feature of nanoparticles of the platinum-group metals prepared by the MVS route. Subsequent characterisation work using electron microscopes with higher resolving power has shown that

many of these particles may be imaged at essentially atomic levels of resolution and the results of this work are described here.

Some general features which have emerged from the HRTEM characterisation of these solvent-stabilised nanoparticles are indicated below. Two distinct typical features are observed when the specimens are examined after deposition of their solutions directly on to lacey carbon films. The first is the preponderance of discrete particles in the size range 1–5 nm which, from the contrast exhibited, appear metallic in nature. A typical example is illustrated in Fig. 1 for a Pd–MeC(O)Et–KD1 preparation. Analysis of several micrographs of the type shown in Fig. 1 gives a palladium particle size distribution shown in Fig. 2(*a*) in which 60 and 30% of the particles are within the size ranges 1.1–2.0 and 2.0–3.0 nm respectively. This distribution compares favourably with, for example, that observed in the more conventional chemical method of preparation of the 'giant palladium clusters' in which *ca.* 25 to 52% of the particles occupy these size ranges[4] [see Fig. 2(*b*)]. Examination of some of the larger individual particles at higher magnifications has provided evidence for a range of face-centred cubic (f.c.c.) octahedral, f.c.c. cuboctahedral and icosahedral metal frameworks.

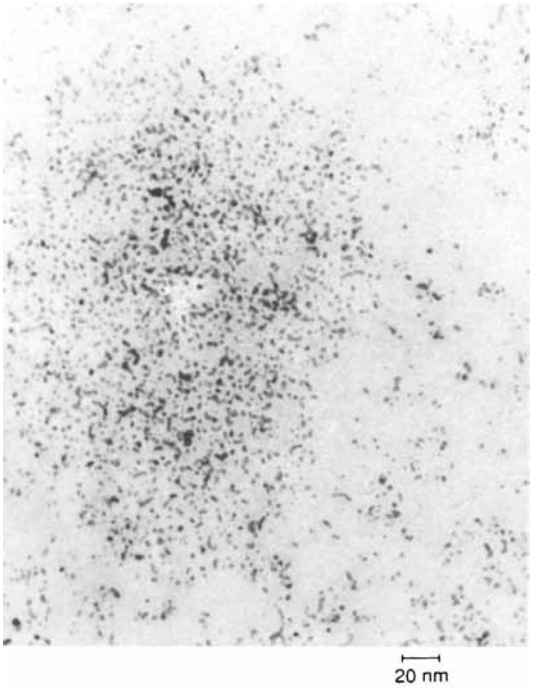


**Fig. 1** Typical electron micrograph of palladium nanoparticles [ex-Pd–MeC(O)Et–KD1] dispersed on lacey carbon film, magnification 200 K

The second common feature relates to the observations of much larger aggregates or assemblies which at low magnifications have been described as 'frogspawn', 'raspberries' or 'caviar' depending upon one's country of origin! At higher magnifications these appear to contain similar small primary particles to those illustrated in Fig. 1 which are held together to form much larger aggregates. Although it is difficult to be quantitative, the overall image contrast observed seems rather less than that observed with the discrete metallic particles, suggesting that some of these aggregates may perhaps contain some organometallic component in addition to purely metallic states. A typical example of this aggregation phenomenon is shown in Fig. 3(*a*) for a Pd–MeC(O)Et–KD2 preparation and an extreme example in Fig. 3(*b*) in which platinum nanoparticles from a platinum–acetone–water preparation have assembled into a 'super-sphere' of cross-section 140 nm. The latter example is unusual and is not typically observed in other nanoparticle preparations. Nevertheless, after use as

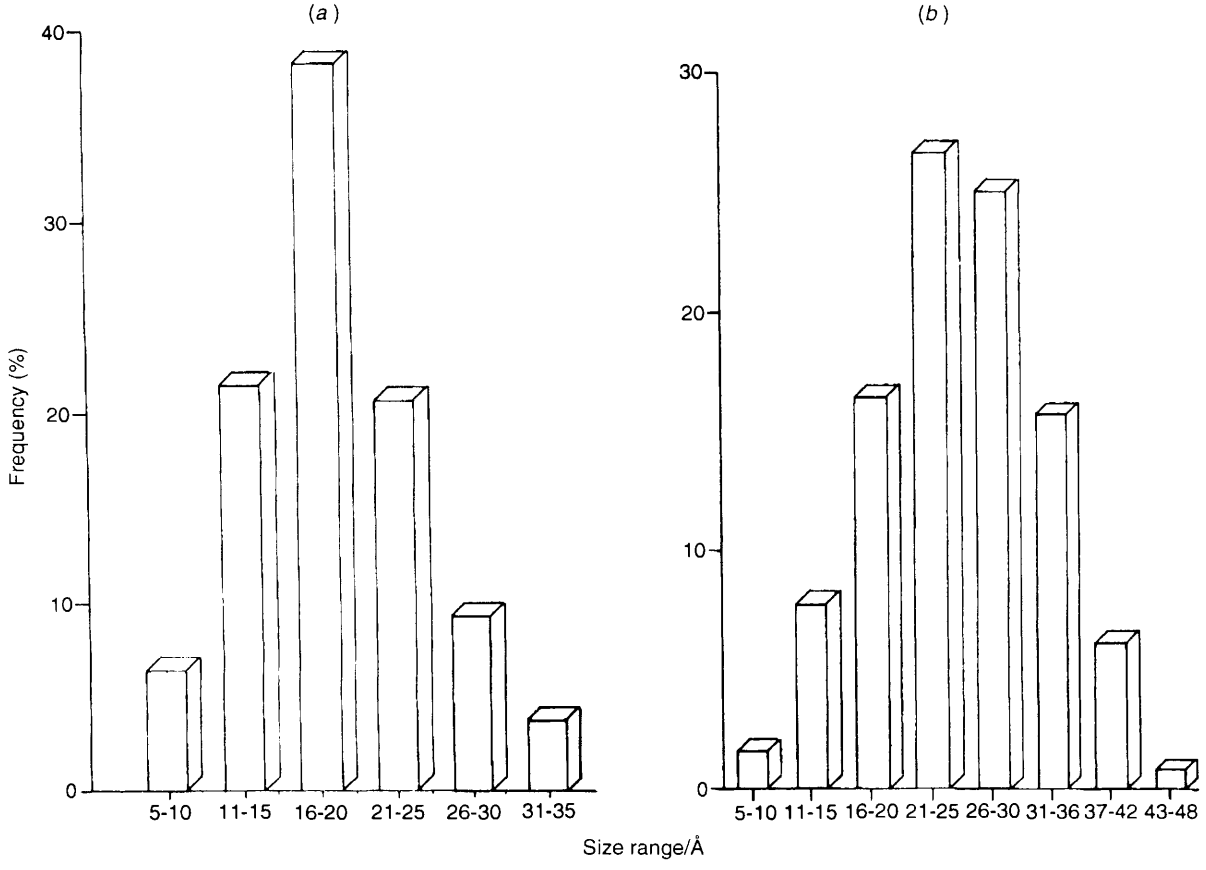


**Fig. 2** Size distribution of (*a*) palladium nanoparticles prepared by MVS, (*b*) 'giant palladium clusters' ex-$Pd_{561}(phen)_{60}(O_2CMe)_{180}$, where phen = 1,10-phenanthroline

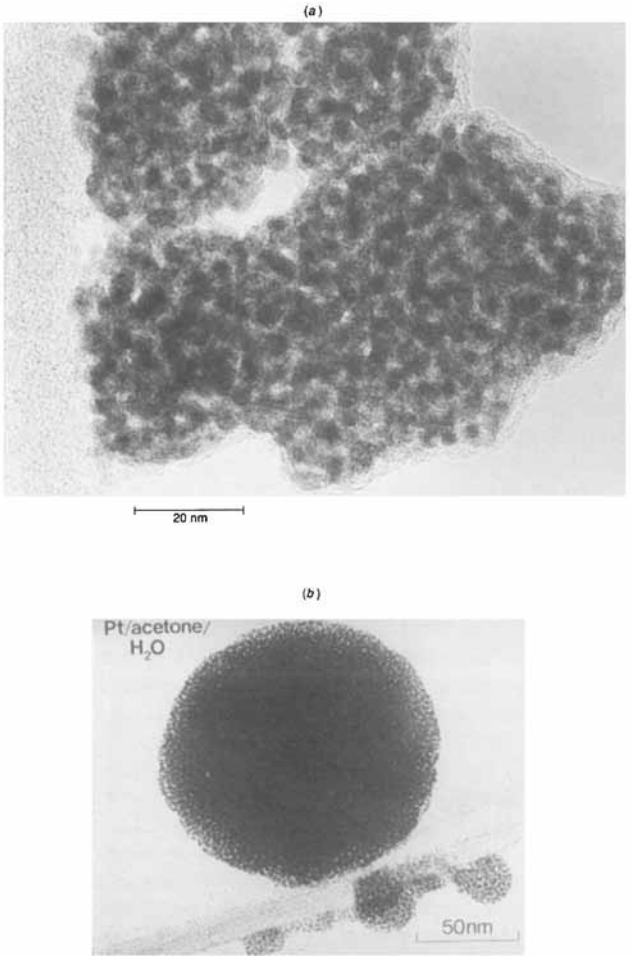


**Fig. 3** (*a*) Typical electron micrograph of 'frogspawn'-type material [ex-Pd–MeC(O)Et–KD2]. (*b*) Extreme example of aggregation into a 'super-sphere' (ex-platinum–acetone–water)

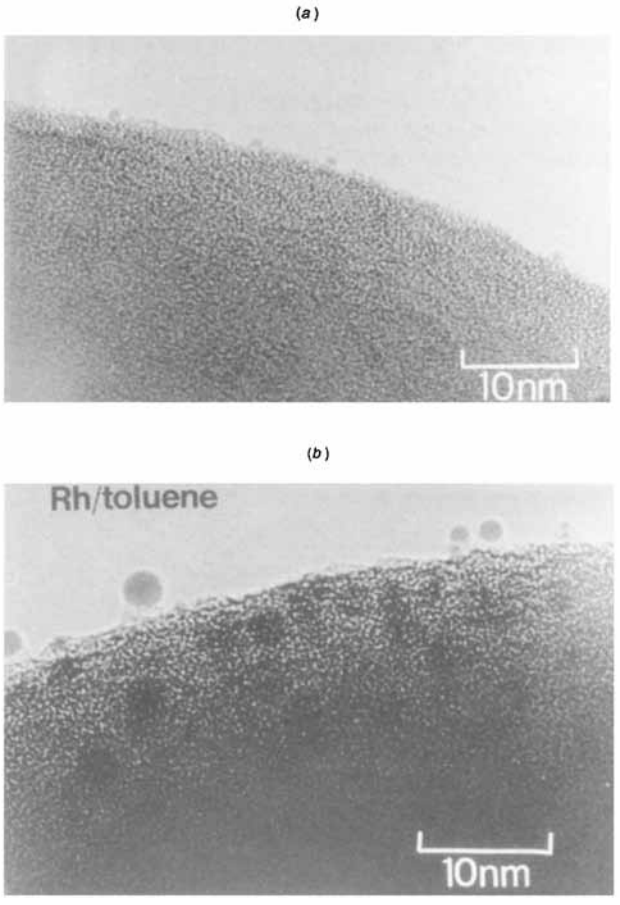


**Fig. 4** Surface profile images of (*a*) platinum nanoparticles, size range 0.8–1.4 nm [ex-Pt–MeC(O)Et–KD2] and (*b*) rhodium nanoparticles (ex-rhodium–toluene), supported on silica microspheres

catalysts for the enantioselective hydrogenation of ethyl pyruvate in the presence of a cinchonidine modifier,[9] the occurrence of large spherical aggregates becomes much more common with both palladium and platinum nanoparticles. This highlights further the ill understood nature of the role of the modifier and solvents in such systems. The relative amounts of discrete metallic particles *vs.* 'frogspawn' vary with the metal but the latter is particularly noticeable in the case of ruthenium nanoparticle preparations.

Close examination of many of the electron micrographs has indicated evidence for the presence of nanoparticles of dimensions less than 1.5 nm which were very difficult to image clearly against the background speckle contrast exhibited by the carbon film. Attempts were therefore made to image the smaller particles in particular by other methods, specifically by profile imaging the particles after dispersion on either silica microspheres of diameter *ca.* 250 nm or MgO smoke cubes. Fig. 4(*a*) and 4(*b*) illustrate examples of platinum [ex-Pt–MeC(O)Et–KD2] and rhodium (ex-rhodium–toluene) nanoparticles respectively obtained by the former approach. In Fig. 4(*a*) several spherically shaped platinum particles in the size range 0.8–1.4 nm are clearly visible; these would have been very difficult if not impossible to detect on the carbon films. For the purposes of perspective, dimensions of 0.8 and 1.4 nm correspond to those expected from the 13 and 55 atom first and second closed-shell clusters respectively.[10] The profile images of rhodium nanoparticles of diameter 0.9, 1.9 and 3.0 nm are shown in Fig. 4(*b*). These diameters correspond approximately to the expected sizes of the first, third and fifth closed-shell cluster configurations containing 13, 147 and 561 metal atoms respectively. These observations may be of significance in the light of the possibility that the outer, non-closed-shell atoms may be highly mobile and therefore less obvious in the image than are the closed-shell atoms. The 3.0 nm particle shows clear evidence of lattice structure. Particles of this type do show a 'quasi-molten' behaviour, the lattice structure apparently moving in and out of register during exposure to the electron beam. This is a common feature and is further exemplified in some examples of palladium particles [ex-Pd–MeC(O)Et–KD1] when profile imaged on MgO smoke cubes (see Fig. 5). These particles of *ca.* 1.9 nm in diameter appear to vibrate about a mean position but do not coalesce with neighbouring particles. They have also been shown to exhibit transient lattice features which correspond to the {111} spacings of palladium almost matched to corresponding spacings of crystalline MgO. On careful inspection of the micrographs the slight curvature which is observed in the base of the palladium particles is consistent with the lattice mismatch between Pd (0.225 nm) and MgO (0.242 nm). Giorgio *et al.*[11] have previously reported lattice accommodation of *in situ* evaporated 5 nm palladium particles at the interface of an MgO support.

Although analytical electron microscopy has been used to determine the ligand : metal ratios of high-nuclearity carbonyl clusters, the ligands are easily lost with increasing beam intensity and exposure times.[12] In spite of repeated attempts it has proved difficult using this technique to obtain information which could clarify the role played by the organic solvents and dispersing agents in the stabilisation of the nanoparticles. Nevertheless, by taking great care to maintain minimum current density, evidence for the existence of what is believed to be an organic coating has been obtained through observation of an amorphous concentric layer surrounding the metallic core when the particles are supported on silica microspheres. This outer layer disappears rapidly with increasing beam-current densities.

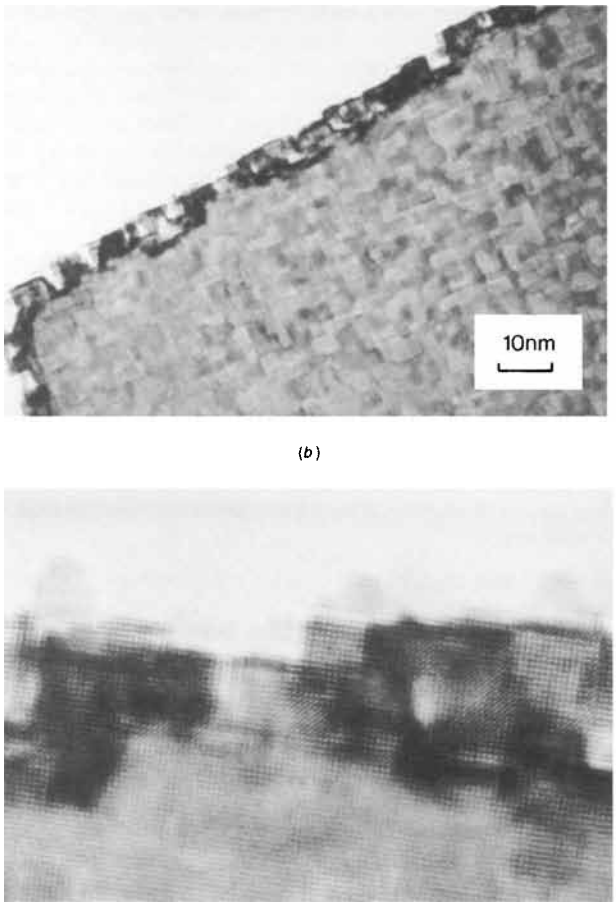


**Fig. 5** Surface profile images of palladium particles, size 1.9 nm, [ex-Pd–MeC(O)Et–KD1] supported on magnesium oxide smoke cubes: (*a*) general view of 110 × 80 nm area, (*b*) close-up of nanoparticles

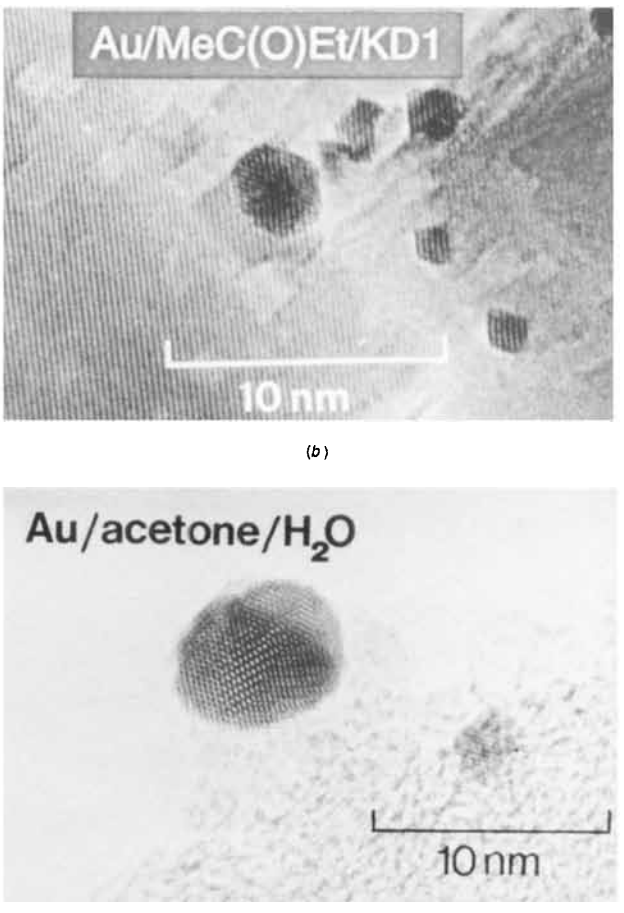


**Fig. 6** (*a*) Octahedral and cuboctahedral gold particles [ex-Au–MeC(O)Et–KD1] exhibiting an epitaxial relationship with the magnesium oxide smoke-cube support; imaged along the [110] direction. (*b*) A 7 nm multiply twinned gold particle [ex-gold–acetone–water]

Solvent-stabilised gold nanoparticles prepared by the MVS route show some significant differences from those of the platinum-group metals. Small particles in the 1–3 nm size range may also be prepared and characterised, as illustrated in Fig. 6(*a*). In this example the nanoparticles derived from Au–MeC(O)Et–KD1, when dispersed on MgO smoke cubes, clearly exhibit an epitaxial relationship with the MgO support material. However, in addition to small particles, these MVS preparations can also result in the formation of much larger particles (up to 20 nm in size) even when the preparations have included dispersing agents. Fig. 6(*b*) illustrates an example of a 7 nm multiply twinned particle obtained from a gold–acetone–water preparation. Moreover in some, but not all, cases the particle sizes have been found to vary with storage, as have the colours of their solutions. Those containing the smallest particles (1–3 nm) are brown whereas those containing particles larger than 5 nm exhibit purple-red colourations and show the plasmon absorption [13,14] characteristic of metallic Au at *ca.* 540 nm in the optical spectrum.

### Concentration-dependent growth phenomenon associated with gold nanoparticles

The particle-growth phenomenon was first observed as a consequence of changes in the colour of some of the solutions from brown to red and/or purple during storage over a period of time. Fig. 7 shows typical examples of the changes occurring in the optical spectra, in particular the growth of the plasmon absorption at *ca.* 540 nm as a function of time. Initially this particle-growth phenomenon appeared to occur almost randomly but careful examination of what is now quite an extensive body of information has allowed the following rationalisations in respect of these Au–MeC(O)Et preparations.

(*i*) Immediately after preparation and warm-up in the MVS reactor brown solutions containing primary particles in the size range 1–4 nm are obtained.

(*ii*) The primary particle size appears to be dependent upon the metal concentration; in general higher concentrations favour larger particle sizes. Rapid warm-up has been found to enhance the relative amounts of smaller particles, possibly by a quenching process.

(*iii*) The use of dispersing agents has little effect on the primary particle sizes but their presence prevents the aggregation/chaining of individual particles, a phenomenon which appears to be associated with the development of blue colours in the solutions.

(*iv*) Below a critical concentration (*ca.* 0.01% w/v) the primary particles are unstable with respect to storage at room temperature. Over a period of weeks larger particles appear to grow at the expense of smaller particles with the concomitant development of red or purple colours. Storage of the solutions at −20 °C significantly slows but does not completely inhibit the rate of particle growth.

(*v*) Above the limiting concentration, *i.e.* >0.01% w/v, the primary particles appear stable with respect to storage at room temperature over a period of months, the solutions remaining brown. However, upon dilution (to below the limiting concentration) by the addition of pure solvent, particle growth is initiated and then occurs at an equivalent rate to that

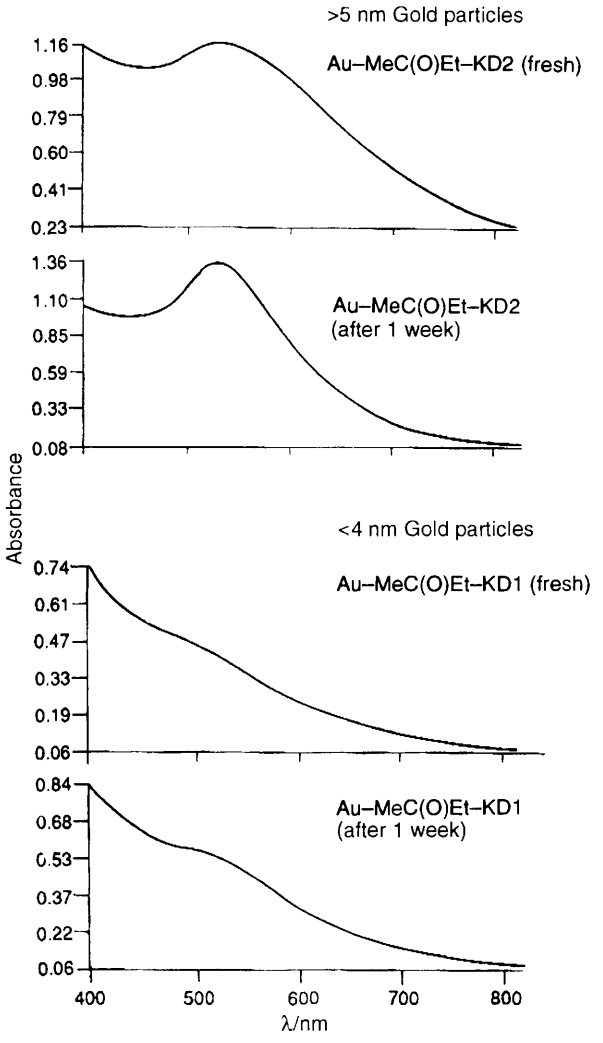


**Fig. 7** Typical optical absorption spectra of gold nanoparticles

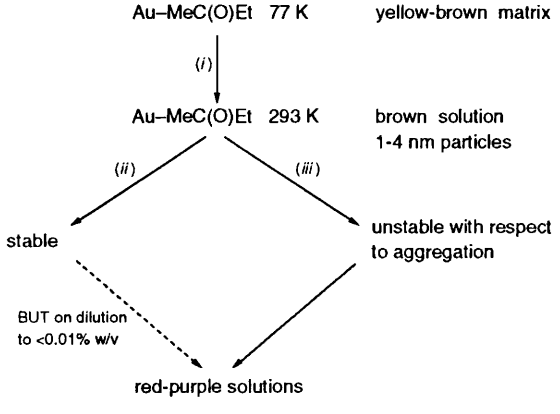


**Scheme 1** Particle growth phenomena. (*i*) Warm-up; (*ii*) > 0.01% w/v Au; (*iii*) < 0.01%, w/v Au

observed with corresponding samples containing the same initial concentrations below 0.01% w/v (see Scheme 1). A parallel change in colour from brown to red (or purple) is also observed. The explanations for these unusual effects are not obvious. For example, one possible explanation concerning desorption of the dispersing agent on dilution can be eliminated because the effect is also observed in the absence of added dispersing agents.

(*vi*) The plasmon absorption at 520–540 nm in the optical spectrum, which is associated with typical preparations of colloidal gold, and which is responsible for their red/purple colours, is not observed in spectra of the freshly prepared materials. As particle growth occurs this band becomes evident and its appearance seems to correspond with the presence of particles > 4 nm in size. However there appears to be no obvious relationship between the measured absorbance of this band and particle size in the range 4–30 nm. This may arise as a consequence of the fact that the larger particles are no longer perfectly spherical but are partially elongated or aggregated and this effect is superimposed on the plasmon band-width size effect.*[15,16] Above 30 nm precipitation of the particles occurs.

(*vii*) Initial experiments with other solvents, *e.g.* acetone, acetone–water mixtures, methylcyclohexane and toluene, indicate that the behaviour described above may be quite general although the detailed parameters are different and require further investigation.

(*viii*) In order to obtain reproducibly 1–3 nm size gold nanoparticles which are stable with respect to aggregation, it is necessary to work above the limiting concentration level of 0.01% w/v and to employ faster rather than slower warm-up techniques.

### Matrix-assisted laser desorption ionisation time-of-flight mass spectrometry

The HRTEM technique has provided much useful information relating to the characterisation of nanoparticle sizes and structures. Nevertheless it does have limitations and is very time and instrument intensive. Access to a simple, relatively rapid and routine physical method which would provide an estimate of molecular weight and hence particle size could provide a significant advance to the progress of work in this area. The recent development of MALDI-TOF mass spectrometry[17,18] provides a relatively simple inexpensive instrument with very high sensitivity and almost unlimited mass range. This technique is now extensively exploited to obtain molecular weights in excess of 300 000 in biological molecules such as proteins, carbohydrates and oligonucleotides.[19] We have applied the technique for the first time to obtain data on nanoparticles.

Fig. 8 shows a MALDI spectrum obtained, using the reflectron attachment, directly from a fresh Au–MeC(O)Et preparation containing particles in the size range 1–2 nm. It shows a broad maximum centred at *m/z* 4857 upon which is superimposed fine structure. Examination of the spectrum in the low-mass range provides unambiguous evidence for the presence of Au. Expansion of the spectrum in Fig. 8(*a*) over the *m/z* range 4500–5500 [Fig. 8(*b*)] shows a series of 13 peaks separated by an average of 73 mass units [the molecular weight of MeC(O)Et is 72]. A MALDI spectrum of the ketone alone gave no peaks in this region. Although the details await full interpretation the spectrum is consistent with an intimate combination of Au and the ketone. Of many possible combinations, it is perhaps significant that species of composition $Au_{21}L_{10}$ and $Au_{13}L_{32}$ [L = MeC(O)Et] have molecular weights in the region of 4850. The first mentioned would be expected to have a particle diameter at the lower end of the size range determined by HRTEM.

A second example concerns the giant palladium cluster[4] of nominal composition $Pd_{561}(phen)_{60}(O_2CMe)_{180}$. As part of a collaborative programme with Professor Moiseev[20] we have previously examined this cluster by HRTEM and confirmed that the majority of the sample falls within the 21–25 and 26–30 Å histogram bars [Fig. 2(*b*)] which, depending upon the assumptions used in deriving the particle diameters, is of the approximate size (25.7–28.5 Å) expected for a $Pd_{561}$ cluster. A MALDI-TOF mass spectrum obtained on this species is illustrated in Fig. 9. It contains a series of broad peaks which may be interpreted in terms of the sequential fragmentation of

* The authors wish to acknowledge a referee for this suggestion.

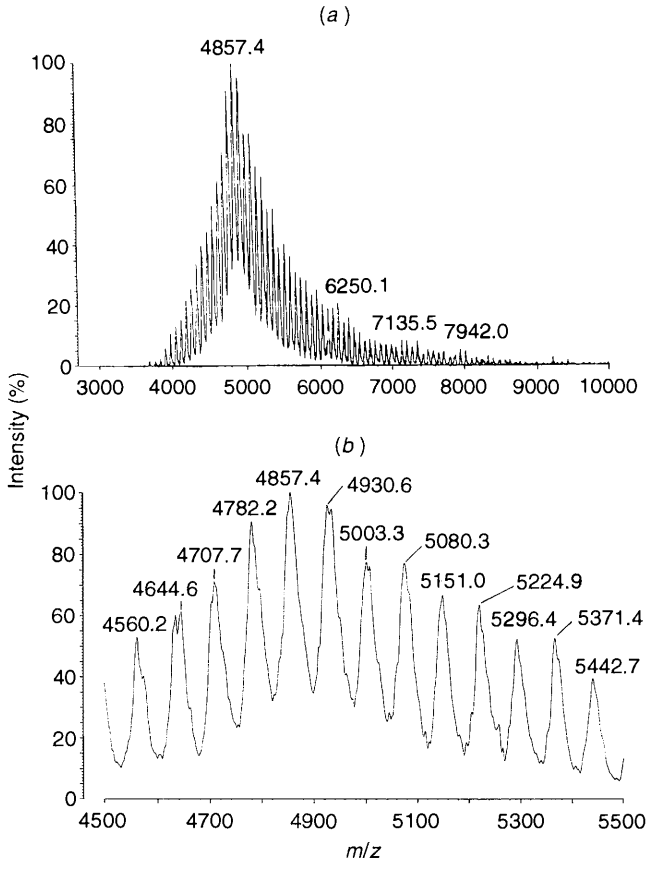


**Fig. 8** (*a*) A MALDI-TOF mass spectrum obtained from gold nanoparticles [ex-Au–MeC(O)Et]; (*b*) expansion of the *m*/*z* 4500–5500 range

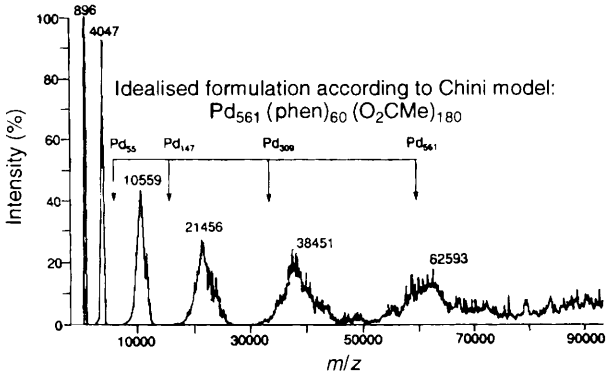


**Fig. 9** A MALDI-TOF mass spectrum obtained from $Pd_{561}(phen)_{60}(O_2CMe)_{180}$

the five-shell cluster (containing some additional ligands), with remarkably good agreement between calculated and observed values of the mass losses associated with $Pd_n$ minus $Pd_{n-1}$ closed-shell configurations, as indicated in Table 2.

Although these are very preliminary results and their interpretation is certainly by no means unambiguous they do provide considerable incentive for the further investigation of MALDI-TOF mass spectrometry in this area of chemistry.

## Conclusion

We have demonstrated that the MVS technique can be used to prepare solvent-stabilised nanoparticles of Ru, Rh, Pd, Pt, Ag and Au in the size regime which encompasses high-nuclearity clusters and typical small colloidal metals and that these can be characterised by HRTEM. In the case of nanoparticulate Au we have identified an unusual concentration-dependent particle-aggregation phenomenon, the explanation for which is presently not obvious.

We have also established a regime of preparative conditions under which 1–3 nm size gold particles, which are stable with respect to aggregation and growth, and which do not display the plasmon absorption characteristic of most colloidal gold preparations, may be produced.

Finally we have obtained preliminary promising evidence for the application of MALDI-TOF mass spectrometry in this area of chemistry.

**Table 2** Fragmentation of giant palladium clusters

| Chini model | | MALDI-TOF mass spectrum |
|---|---|---|
| $Pd_n$–$Pd_{n-1}$ | $M_{calc}$ | $M_{found}$ |
| 561 309 | 26 813 | 24 000 |
| 309–147 | 17 237 | 17 000 |
| 147–55 | 9 789 | 11 000 |
| 55–13 | 4 469 | 6 500 |

## Acknowledgements

We wish to thank the Royal Society–SERC for an Industrial Fellowship (to R. W.), the SERC Nanotechnology Initiative, Grant ref. GR/H71635 (T. G.) and Kratos Analytical (Drs. W. Richardson, M. Kimber and colleagues) for access to the Kompact MALDI 3 mass spectrometer. We also thank Professor I. I. Moiseev and Dr. M. N. Vargaftik for the sample used to obtain Fig. 9.

## References

1 P. P. Edwards, *Mater. Res. Soc. Symp. Proc.*, 1992, **272**, 311 and refs. therein.
2 A. Ceriotti, F. Demartin, G. Longoni, M. Manassero, M. Marchionna, G. Piva and M. Sansoni, *Angew. Chem., Int. Ed. Engl.*, 1985, **24**, 697.
3 G. Schmid, *Chem. Rev.*, 1992, **92**, 1709.
4 M. N. Vargaftik, I. I. Moiseev, D. I. Kochubey and K. I. Zamaraev, *Faraday Discuss. Chem. Soc.*, 1991, **92**, 13.
5 M. Brust, M. Walker, D. Bethell, D. J. Schiffrin and R. Whyman, *J. Chem. Soc., Chem. Commun.*, 1994, 801.
6 G. A. Ozin, M. P. Andrews, C. G. Francis, H. X. Huber and K. Molnar, *Inorg. Chem.*, 1990, **29**, 1068.
7 S.-T. Lin, M. T. Franklin and K. J. Klabunde, *Langmuir*, 1986, **2**, 259.
8 A. F. Simpson, J. A. Stott and R. Whyman, unpublished work.
9 P. J. Collier, T. Goulding, J. A. Iggo and R. Whyman, *Chiral Reactions in Heterogeneous Catalysis*, eds. G. Jannes and V. Dubois, Plenum, New York, 1995, p. 105.
10 B. K. Teo and N. J. A. Sloane, *Inorg. Chem.*, 1985, **24**, 4545.
11 S. Giorgio, C. R. Henry, C. Chapon and G. Nihoul, *Philos. Mag. B*, 1993, **67**, 73.
12 R. W. Devenish, S. Mulley, B. T. Heaton and G. Longoni, *J. Mater. Res.*, 1992, **7**, 2810.
13 W. P. Halperin, *Rev. Mod. Phys.*, 1986, **58**, 533.
14 J. A. Creighton and D. G. Eadon, *J. Chem. Soc., Faraday Trans.*, 1991, 3881.
15 U. Kreibig and L. Genzel, *Surf. Sci.*, 1985, **156**, 678.
16 D. G. Duff, A. Baiker and P. P. Edwards, *Langmuir*, 1993, **9**, 2301.
17 M. Karas and F. Hillenkamp, *Anal. Chem.*, 1988, **60**, 2299.
18 K. Tanaka, H. Waki, Y. I. Ido, S. Akita, Y. Yoshida and T. Yoshida, *Rapid Commun. Mass Spectrom.*, 1988, **2**, 151.
19 R. J. Cotter, *Anal. Chem.*, 1992, **64**, 1027A.
20 F. Cea, R. W. Devenish, B. T. Heaton, I. I. Moiseev, A. K. Smith, J. Temple, M. N. Vargaftik and R. Whyman, unpublished work.

*Received* 31*st July* 1995; *Paper* 5/06314K